

# Synergistic Effect of Tungsten Nitride and Palladium for the Selective Hydrogenation of Cinnamaldehyde at the C=C bond

Dong Wang,<sup>[a, b]</sup> Yujun Zhu,<sup>\*[a]</sup> Chungui Tian,<sup>[a]</sup> Lei Wang,<sup>[a]</sup> Wei Zhou,<sup>[a]</sup> Yongli Dong,<sup>[a]</sup> Haijing Yan,<sup>[a]</sup> and Honggang Fu<sup>\*[a]</sup>

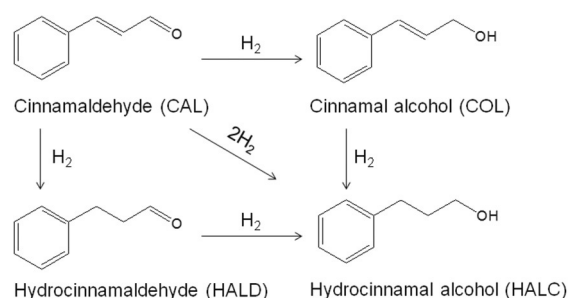
Herein, a series of catalysts made of Pd–WN on various supports was synthesized by modifying supports with small-size WN NPs firstly and loading Pd subsequently. Their catalytic performances were evaluated for selective hydrogenation of cinnamaldehyde (CAL) to hydrocinnamaldehyde (HALD). Interestingly, it was found the synergistic effect between Pd and WN can improve conversion and selectivity of CAL to HALD. Among these catalysts, Pd–WN/SBA-15 shows best performance with highest conversion (99%) and selectivity to

HALD (97%), which is superior to commercial 5% Pd/C catalyst. The hydrogenation kinetics of Pd–WN/SBA-15 has been adequately represented by a standard pseudo-first-order approximation, and it discloses that the existence of WN can effectively decrease the activation energy (23.2 kJ mol<sup>-1</sup>). The synergistic effect of Pd and WN results in enriching the electron density of Pd, increasing the ratio of surface Pd<sup>0</sup> and decreasing the size of Pd on the Pd–WN/SBA-15 catalyst.

## Introduction

The hydrogenation of  $\alpha,\beta$ -unsaturated aldehydes to  $\alpha,\beta$ -unsaturated alcohols or saturated aldehydes is a critical step in the synthesis of a large number of fine chemicals, such as pharmaceuticals, perfumes, and food additives.<sup>[1–3]</sup> Recently, hydrocinnamaldehyde (HALD) was found to be an important intermediate in the synthesis of pharmaceuticals used in the treatment of HIV.<sup>[4]</sup> Cinnamaldehyde (CAL), as typical  $\alpha,\beta$ -unsaturated aldehyde, can result in various product distributions in its hydrogenation route (Scheme 1), depending on the active metal, solvent, and promoter. In general, Pd catalysts are in favor of the hydrogenation of the C=C bond to produce HALD, and Pt-based catalysts facilitate the production of cinnamyl alcohol (COL) through the hydrogenation of the C=O bond.<sup>[5]</sup> Although the reduction of the C=C group is favored thermodynamically,<sup>[6–11]</sup> it is still challenging to enhance the efficiency of Pd catalysts and lessen Pd usage.<sup>[12,13]</sup>

In recent years, metal nitrides have been studied intensely owing to their synergistic effects and Pt-like behavior in tradi-



Scheme 1. Reaction pathways for cinnamaldehyde hydrogenation.

tional catalysis and electrocatalysis.<sup>[14–16]</sup> It has been proven that tungsten and tungsten nitride are effective co-catalysts of Pt and Pd in hydrogen evolution reaction and oxygen reduction reaction.<sup>[15,17,18]</sup> Importantly, in our previous work it was found that Mo<sub>2</sub>N could distinctively enhance the activity and selectivity of Pt on the ternary Pt–Mo<sub>2</sub>N/SBA-15 catalyst for the hydrogenation of CAL at the C=O bond to COL. Thus, we were curious to investigate whether the synergistic effect between Pd and WN could promote the catalytic performance of Pd for the hydrogenation of cinnamaldehyde at the C=C bond to HALD.

To strengthen the interaction of Pd and WN, it is essential to gain small-sized and highly dispersed WN nanoparticles (NPs) to increase the opportunity of WN contacting with Pd. Thanks to our successful strategy to support small-size Mo<sub>2</sub>N NPs on SBA-15,<sup>[19]</sup> on various supports with Si–OH and Al–OH groups, we considered it more effective to use *N*-[3-(trimethoxysilyl)propyl]-ethylenediamine with two amino groups as a silane coupling agent to immobilize H<sub>4</sub>[SiO<sub>4</sub>(W<sub>3</sub>O<sub>9</sub>)<sub>4</sub>](SiW<sub>12</sub>) clusters and obtain tiny WN NPs after calcination in pure NH<sub>3</sub>.

[a] D. Wang, Prof. Y. Zhu, Prof. C. Tian, Dr. L. Wang, Prof. W. Zhou, Y. Dong, H. Yan, Prof. H. Fu  
Key Laboratory of Functional Inorganic Material Chemistry  
Heilongjiang University  
Ministry of Education; School of Chemistry and Materials  
Heilongjiang University  
74 Xuefu Road, Harbin 150080 (P.R. China)  
E-mail: fuhg@vip.sina.com  
yujunzhu@hlju.edu.cn

[b] D. Wang  
School of Chemical and Environmental Engineering  
Hanshan Normal University  
Chaozhou 521041 (P.R. China)

Supporting Information for this article can be found under <http://dx.doi.org/10.1002/cctc.201600184>.

Based on above discussion, a series of ternary Pd–WN catalysts on different supports were prepared by loading Pd on WN-modified supports. These ternary catalysts showed superior performance over the binary catalysts without WN for the hydrogenation of CAL at the C=C bond; and Pd–WN/SBA-15 displayed the best selectivity to HALD with near 100% conversion of CAL. The intrinsic synergistic effect between Pd and WN was explored by investigating the influence of WN on the structure, the hydrogenation kinetics, and the stability of the Pd–WN/SBA-15 catalyst. It was found that the addition of WN enriched the electron density of Pd, increased the ratio of Pd<sup>0</sup> species, and greatly decreased Pd NPs size, which led to the enhanced performance, lower active energy, and good stability. In this work, we extend our previous work to the scope of synergistic effect between noble metal and nitrides on the hydrogenation of CAL at the C=C bond to HALD. The study gives a further insight to the nature of the synergistic effect between noble metal and nitrides.

## Results and Discussion

The catalytic performances were investigated for the selective hydrogenation of CAL over various catalysts including 1.5% Pd–WN/SBA-15, 1.5% Pd–WN/MCM-41, 1.5% Pd–WN/Na-Beta, 0.75% Pd–WN/Al<sub>2</sub>O<sub>3</sub>, and 1.5% Pd–WN/SAPO-34 catalysts. The results are listed in Table S1 in the Supporting Information. It was found that HALD was the main product for all catalysts; however, CAL conversion and selectivity to HALD were different owing to the difference in the natures of supports. Notably, the ternary catalysts with different supports showed higher conversion and selectivity than the binary ones without WN. Especially, for the 1.5% Pd–WN/SBA-15 catalyst, the selectivity to HALD attained to 97.6%, corresponding 99.5% conversion of CAL, which was superior to that of commercial 5% Pd/C catalyst. Evidently, WN plays an important role in enhancing the activity and selectivity of Pd NPs on various catalysts. This result illustrates that the WN had a positive effect on Pd for the selective hydrogenation of cinnamaldehyde at the C=C bond. To clarify what the nature of the synergistic effect of Pd and WN is, 1.5% Pd–WN/SBA-15 was taken as a typical catalyst to investigate its structure and catalytic property.

### Characterization of Pd–WN/SBA-15

The low-angle XRD patterns are displayed in Figure 1 for 1.5% Pd–WN/SBA-15 and the reference samples including SBA-15,

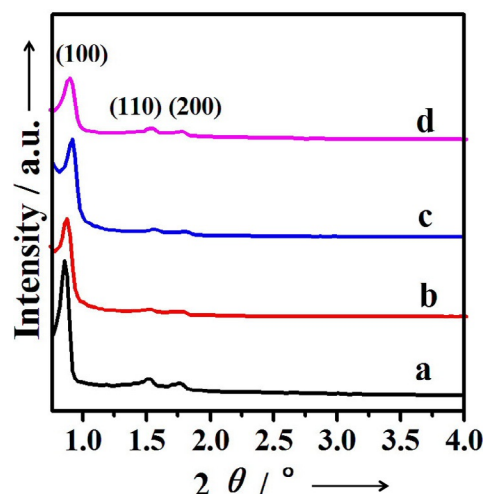


**Figure 1.** Low-angle XRD patterns of a) SBA-15, b) 1.5% Pd/SBA-15, c) WN/SBA-15, and d) 1.5% Pd–WN/SBA-15.

WN/SBA-15, and 1.5% Pd/SBA-15 samples. In Figure 1, all the samples exhibited prominent peaks corresponding to (100), (110), and (200) reflection at  $2\theta$  approximately  $0.5\text{--}2^\circ$ , which is characteristic of the hexagonal mesostructure of the SBA-15 host (Figure 1a).<sup>[20–22]</sup> This indicates that the loads of WN and Pd do not destroy the well-ordered mesoporous structure of SBA-15. However, the intensity of the (100) reflection showed a clear decrease for WN/SBA-15 and 1.5% Pd–WN/SBA-15, which depicts the decrease in the mesoporous ordering of SBA-15. Moreover, compared with the pure SBA-15, the (100) reflections of WN/SBA-15 and 1.5% Pd–WN/SBA-15 sample shift to higher angles, indicating that WN and Pd NPs are scattered into the pore channels of SBA-15.

The textural properties of the samples have been also disclosed by N<sub>2</sub> adsorption–desorption analysis as listed in Table 1 and Figure S1 (Supporting Information), including WN/SBA-15, 1.5% Pd–WN/SBA-15, and 1.5% Pd/SBA-15. As expected, a significant decrease in the surface area of all samples was observed upon metal loading. Pore sizes were reduced for the samples of WN/SBA-15 and 1.5% Pd–WN/SBA-15, which was consistent with the low-angle XRD results. Pore volumes also followed the similar trend, which indicates that nanoparticles are dispersed within the pores of SBA-15.

The morphologies of the WN/SBA-15 and 1.5% Pd–WN/SBA-15 were unambiguously characterized by TEM. The TEM image for WN/SBA-15 composite (Figure 2a,b) clearly depicted a fairly

**Table 1.** Relevant physicochemical parameters of the different samples.

| Sample                             | $S_{\text{BET}}$ [m <sup>2</sup> g <sup>−1</sup> ] <sup>[a]</sup> | $V_{\text{pore}}$ [cm <sup>3</sup> g <sup>−1</sup> ] <sup>[a]</sup> | Pore size [nm] <sup>[a]</sup> | $d_{\text{TEM}}$ [nm] <sup>[b]</sup> | Pd content [wt %] <sup>[c]</sup> |
|------------------------------------|---|---|-------------------------------|--------------------------------------|----------------------------------|
| SBA-15                             | 811   | 1.20  | 8.2                           | –                                    | –                                |
| WN/SBA-15                          | 468   | 0.69  | 6.8                           | 13.6/WN                              | –                                |
| 1.5% Pd–WN/SBA-15                  | 394   | 0.64  | 5.9                           | 16.8                                 | 1.38                             |
| 1.5% Pd/SBA-15                     | 644   | 0.98  | 6.5                           | 12.2/Pd                              | 1.42                             |
| 1.5% Pd–WN/SBA-15-r <sup>[d]</sup> | 403   | 0.65  | 5.8                           | 16.4                                 | 1.29                             |

[a] Derived from N<sub>2</sub> adsorption–desorption isotherms. [b] Average particle sizes calculated from at least 100 individual crystallites in TEM images. [c] The content of Pd determined by ICP–OES. [d] 1.5% Pd–WN/SBA-15 sample after five consecutive catalytic runs.

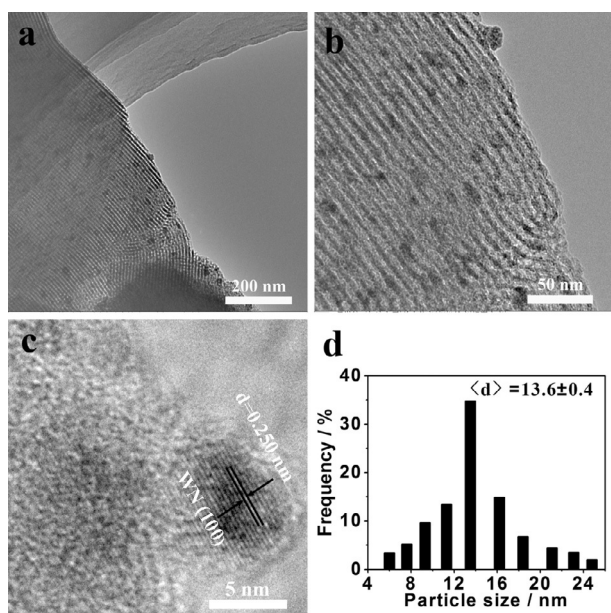


**Figure 2.** a, b) Low-magnification TEM images, c) HRTEM, and d) particle-size distribution of the WN/SBA-15. The histogram in (d) depicts the particle-size distribution and the average size of the particles determined by statistical analysis of the TEM images, at least 100 individual crystallites were analyzed.

good dispersion of tiny nanoparticles on the highly ordered 2D hexagonal mesostructure of SBA-15 with an average particle size of 13.6 nm. In the high-resolution (HR) TEM image (Figure 2c), the crystal plane spacing was measured as 0.250 nm, corresponding to the (100) crystal facet of the hexagonal WN. In addition, SEM element maps for WN/SBA-15 composite (Figure S2) also showed the uniform dispersion of WN on SBA-15. No observable sintering could be found on WN/SBA-15, although the WN content was approximately 8.9% according to the analysis of inductively coupled plasma optical emission spectroscopy (ICP-OES) and X-ray fluorescence analysis. In general, the nitrides show large sizes above micrometer if they are prepared by solid-state ion-exchange route.<sup>[23]</sup> Bazarjani and co-workers have loaded WN NPs on porous silicon oxycarbonitride matrices.<sup>[24]</sup> The as-prepared nitrides have a large size of approximately 40 nm, and their distribution on the support is not uniform. In this work, the obtained WN/SBA-15 sample with small sizes and good dispersion of WN particles was contributed to the small size close to the nanometer and stable structure of  $\text{SiW}_{12}$  clusters, the anchoring function of *N*-[3-(trimethoxysilyl)propyl]-ethylenediamine to  $\text{SiW}_{12}$  clusters, and the mesoporous structure of the SBA-15 support. Thus, the obtained small-size WN NPs possesses more chance to touch with Pd.

For the 1.5% Pd–WN/SBA-15 sample, the TEM image also showed homogeneous dispersion (Figure 3a), but the average particle size increased to 16.8 nm (Figure 3b). Although it is difficult to distinguish Pd from WN in TEM owing to their similar appearance as dark spots in Figure 3a, it can be concluded that the Pd NPs are uniformly dispersed on the WN/SBA-15 composite by corresponding element maps shown in Figure S3. Moreover, from the HRTEM image of 1.5% Pd–WN/SBA-

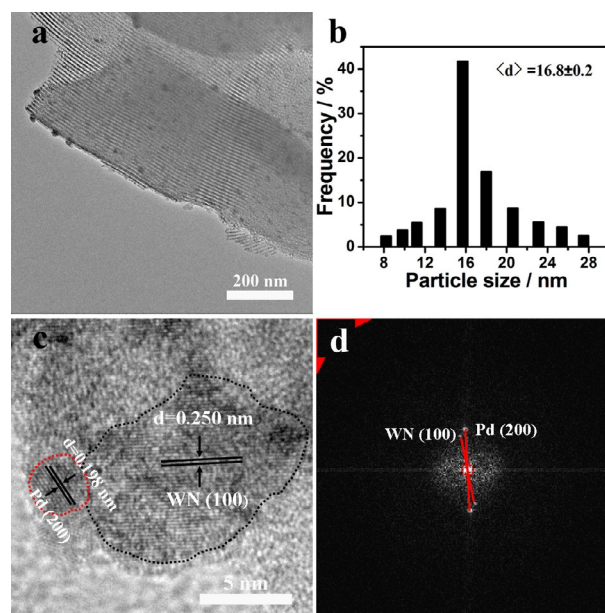


**Figure 3.** a) Low-magnification TEM images, b) particle-size distribution, c) HRTEM, and d) FFT image of the 1.5% Pd–WN/SBA-15. The histogram in (b) depicts the particle-size distribution and the average size of the particles determined by statistical analysis of the TEM images, at least 100 individual crystallites were analyzed.

15 in Figure 3c, it can be seen that WN and Pd were in close contact with each other on the SBA-15. The large particles were typical WN grains with the size of about 12 nm, whereas the relatively small ones located around the WN grains can be ascribed to Pd particles with the (200) crystal plane. The fast Fourier transform (FFT) image (Figure 3d) confirms they are indeed WN with (100) facet and Pd with (200) facet. Thus, the images reveal the coexistence of Pd and WN on 1.5% Pd–WN/SBA-15 catalyst. Notably, the images distinctly show the intimate contact of Pd with WN, which could result in intensive interaction. For the 1.5% Pd/SBA-15, the TEM image (Figure S4) displayed polydispersity and the average particle size was 12.2 nm; even some much larger Pd particles of about 30 nm were seen, indicating the sintering or aggregation of Pd particles in this catalyst. The sintering of pure Pd catalyst has been found in previous reports by Abate et al. and Yang et al.<sup>[25,26]</sup> In view of the TEM images for 1.5% Pd–WN/SBA-15 and 1.5% Pd/SBA-15 catalyst, it can be concluded that the particle size and dispersion of Pd can be controlled effectively by the modification of WN NPs on SBA-15. This effect discloses the intensive interaction between Pd and WN owing to their similar electronic structures.<sup>[16,27]</sup> In addition, the interaction of the nitrides (carbides) with Pt has been discovered in our earlier works by experiments and DFT calculations.<sup>[17,19,28]</sup> Therefore, it is rational to suggest that the Pd NPs are before growing around the highly dispersed WN grains on SBA-15. This point was proven by the increase of the average particle size from 13.6 nm for WN/SBA-15 composite to 16.8 nm for 1.5% Pd–WN/SBA-15 sample.

The compositions of the WN/SBA-15 and 1.5% Pd–WN/SBA-15 were investigated by using wide-angle XRD and the pat-

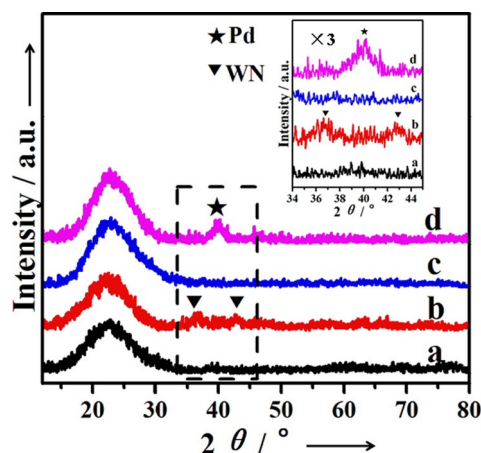


**Figure 4.** Wide-angle XRD patterns and enlarged regional patterns between 34° and 45° (inset) for a) SBA-15, b) WN/SBA-15, c) 1.5% Pd-WN/SBA-15, and d) 1.5% Pd/SBA-15.

terns are shown in Figure 4. The XRD patterns showed a diffuse peak of amorphous SiO<sub>2</sub> at approximately 22.5° for all samples as pure SBA-15 (Figure 4a). For WN/SBA-15 (Figure 4b), the peaks at 37.34 and 43.67° were assigned to the (100) and (101) planes of hexagonal WN. The broad and weak WN diffraction peaks indicate that the WN particles are well dispersed on the composites as displayed in the TEM image (Figure 2a).

After loading Pd, the peaks belonging to WN disappeared in the XRD pattern for the 1.5% Pd-WN/SBA-15. Furthermore, the diffraction peak ascribed to Pd was no longer observed, and the Pd content was 1.38% analyzed by ICP-OES (Table 1). However, for the 1.5% Pd/SBA-15 (Figure 4d), the diffraction peak was clearly observed indexed as Pd (111) planes of a face-centered cubic (fcc) structure at 39.7°, and the Pd content was approximately 1.42%. Compared with 1.5% Pd/SBA-15, the absence of the Pd peak for 1.5% Pd-WN/SBA-15 implies that the existence of WN improves the dispersion of Pd on the SBA-15 support, which is consistent with the results revealed by TEM. This result is also similar to the earlier works.<sup>[17,19]</sup> Although the high surface area of SBA-15 is helpful for getting a high dispersion of Pd, it is evident that WN NPs play a significant role in improving the Pd dispersion and decreasing the particle size of Pd. The enhanced dispersion of Pd reflects that there is intensive interaction between WN and Pd NPs. In addition, contrasted to WN/SBA-15, the disappearance of WN peaks for the 1.5% Pd-WN/SBA-15 also suggests this strong interaction.

To gain further insight into the surface structure of the catalyst, X-ray photoelectron spectroscopy (XPS) analysis was conducted and the results are shown in Figure 5 and Figure 6, together with their deconvolution obtained by fitting Gaussian peaks after Shirley background subtraction. As shown in Figure 5, the Pd XPS spectra of 1.5% Pd-WN/SBA-15 and 1.5% Pd/SBA-15 presented a doublet corresponding to Pd3d<sub>5/2</sub> and Pd3d<sub>3/2</sub>, and the corresponding binding energies (BE) are listed in Table 2. For 1.5% Pd-WN/SBA-15, the Pd3d<sub>5/2</sub> peak at 335.3 eV was described to Pd<sup>0</sup> (metallic palladium),

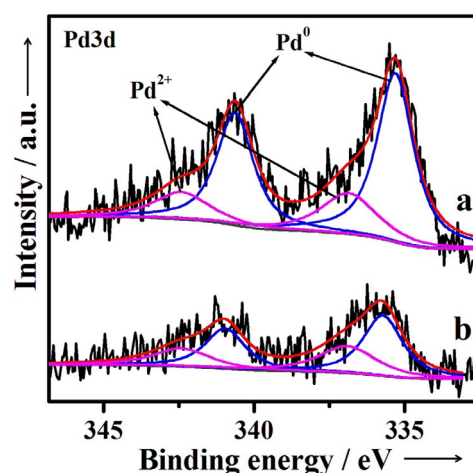


**Figure 5.** Pd 3d XPS spectra of a) 1.5% Pd-WN/SBA-15 and b) 1.5% Pd/SBA-15.

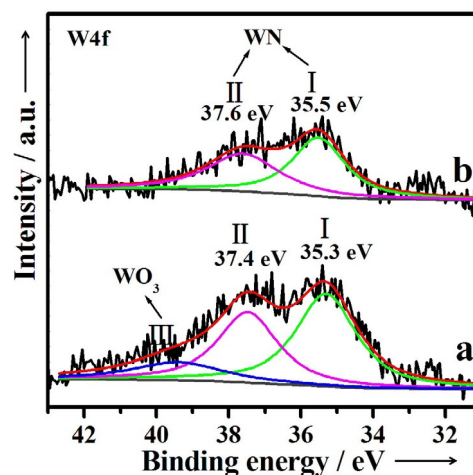


**Figure 6.** W 4f XPS spectra of a) WN/SBA-15 and b) 1.5% Pd-WN/SBA-15.

**Table 2.** XPS data of the Pd 3d levels for the different samples.

| Sample              | Pd species       | Pd species BE [eV] |                   | Content of Pd species [%] |
|---------------------|------------------|--------------------|-------------------|---------------------------|
|                     |                  | 3d <sub>5/2</sub>  | 3d <sub>3/2</sub> |                           |
| 1.5% Pd-WN/SBA-15   | Pd <sup>0</sup>  | 335.3              | 340.6             | 74                        |
|                     | Pd <sup>2+</sup> | 336.8              | 342.3             | 26                        |
| 1.5% Pd/SBA-15      | Pd <sup>0</sup>  | 335.7              | 341.0             | 61                        |
|                     | Pd <sup>2+</sup> | 336.9              | 342.4             | 39                        |
| 1.5% Pd-WN/SBA-15-r | Pd <sup>0</sup>  | 335.0              | 340.3             | 70                        |
|                     | Pd <sup>2+</sup> | 336.4              | 341.9             | 30                        |

and the Pd3d<sub>5/2</sub> peak at 336.8 eV was described to Pd<sup>2+</sup> (palladium oxide) (Figure 5a).<sup>[29]</sup> However, for 1.5% Pd/SBA-15 (Figure 5b), the peak at approximately 335.7 eV was attributed to Pd<sup>0</sup>, and the peak at approximately 336.9 eV corresponded to Pd<sup>2+</sup> species. Thus, on one hand, there is a shift of 0.4 eV toward low binding energy for 1.5% Pd-WN/SBA-15 with respect to 1.5% Pd/SBA-15, which is ascribed to electron transfer between WN and Pd.<sup>[19,30]</sup> Interestingly, this electron transfer

was also proven by the shift of W4f BE for the WN/SBA-15 composite after the load of Pd. For WN/SBA-15 (Figure 6a), the peak of W from W–N located at 35.3 and 37.4 eV and the peak at 39.6 eV were assigned to  $\text{WO}_3$ , indicating low amount or amorphous characteristics of  $\text{WO}_3$  on the surface.<sup>[17]</sup> However, the W4f BEs from W–N for ternary 1.5% Pd–WN/SBA-15 are 35.5 and 37.6 eV (Figure 6b). Clearly, there is a positive shift (0.2 eV) relative to that of WN/SBA-15, confirming the electron transfer from WN to Pd. This transfer is favorable to the increase of the metallic characteristics of Pd by enriching Pd electron density, and the strong electronic interaction can therefore influence catalytic behavior.<sup>[31,32]</sup>

On the other hand, the XPS results also revealed the change of Pd species caused by the interaction between Pd and WN on the 1.5% Pd–WN/SBA-15 surface. The relative abundance of the  $\text{Pd}^0$  (%) species of the samples has been estimated by considering the deconvolution peaks of Pd3d BE. As listed in Table 2, the content of metallic  $\text{Pd}^0$  increased from 61% for 1.5% Pd/SBA-15 to 74% for 1.5% Pd–WN/SBA-15. It also suggests the strengthening of metallic characteristics of Pd in 1.5% Pd–WN/SBA-15. Evidently, the nitride (carbide) could largely improve the crystallinity of the noble metal because of the intensive interaction of nitride (carbide) with noble metal.<sup>[17,28]</sup>

### Selective hydrogenation of CAL by Pd–WN/SBA-15

According to Table S1, 1.5% Pd–WN/SBA-15 showed superior performance for the selective hydrogenation of cinnamaldehyde, and the activity of Pd–WN/SBA-15 with lower Pd content (0.75%) was also studied with WN/SBA-15 and 1.5% Pd/SBA-15 as reference. As listed in Table 3, WN/SBA-15 gave trace conversion (6.9%) of CAL, and CAL was mostly converted to the side products (89.2%), indicating that WN shows poor activity in the hydrogenation process. For 1.5% Pd/SBA-15, it performed 76.9% CAL conversion and 51.5% selectivity to HALD, whereas the selectivity to COL and HALC was 0.8% and 38.9%, respectively. It can be seen that 1.5% Pd/SBA-15 facilitates the production of completely hydrogenated hydrocinnamyl alcohol. However, 0.75% Pd–WN/SBA-15 displayed 70.6% CAL conversion and 89.5% selectivity to HALD. This activity competes

with that of 1.5% Pd/SBA-15. However, it showed much higher TOF ( $757 \text{ h}^{-1}$ ) and selectivity than that over 0.75% Pd/SBA-15 ( $451 \text{ h}^{-1}$ ) and 1.5% Pd/SBA-15 ( $418 \text{ h}^{-1}$ ). In other words, the existence of WN successfully increases the catalytic efficiency of Pd on 0.75% Pd–WN/SBA-15. Herein, it further confirms that the intensive interaction between Pd and WN favors the promotion of the catalytic performance of Pd, and the WN as co-catalyst could lessen the usage of Pd for the selective hydrogenation of CAL in some extent. This effect was also found for Pd and  $\text{Mo}_2\text{N}$  for 1.5% Pd– $\text{Mo}_2\text{N}$ /SBA-15 (Table 3). The CAL conversion and selectivity to HALD was 88.7% and 80.8% over 1.5% Pd– $\text{Mo}_2\text{N}$ /SBA-15, respectively. Clearly, the activity and selectivity of 1.5% Pd– $\text{Mo}_2\text{N}$ /SBA-15 is higher than that of 1.5% Pd/SBA-15 without  $\text{Mo}_2\text{N}$ , which indicates the universality of the enhancement between Pd and different nitrides.

The enhancement of conversion is related to the intensive interaction of Pd and WN, which changes the surface electronic structure of Pd as disclosed by XPS. Compared with 1.5% Pd/SBA-15, the 1.5% Pd–WN/SBA-15 possesses more  $\text{Pd}^0$  species with higher electron density on surface. It is well known that the metallic Pd with high electron density would accelerate its performance on chemoselective hydrogenation of  $\alpha,\beta$ -unsaturated carbonyls.<sup>[33]</sup>

Thus, the conversion rate of CAL was varied by the interaction of Pd and WN. Given the same reaction conditions, the 1.5% Pd–WN/SBA-15 (Figure 7a) showed faster conversion rate of CAL than the 1.5% Pd/SBA-15 (Figure 7b): it took 41 and 61 min to obtain a conversion of 50% for the 1.5% Pd–WN/SBA-15 and 1.5% Pd/SBA-15, respectively. In addition, for the 1.5% Pd–WN/SBA-15, the selectivity to HALD slowly increased from 90.6% at 10 min to 97.6% at 2 h, and the selectivity to COL and HALC was distinctly lower than to HALD. However, for 1.5% Pd/SBA-15, the selectivity to HALD reached 59.5% at the beginning, and slowly decreased to 51.5% subsequently; at the same time, the selectivity to HALC slowly rose up to 38.9%. Very little COL was detected at the present hydrogenation conditions for the both catalyst, similarly to what was previously reported on Pd catalysts.<sup>[34,35]</sup> It can be seen that 1.5% Pd/SBA-15 could convert more CAL to saturated alcohol (HALC) than the 1.5% Pd–WN/SBA-15, which induces the decrease of the selectivity to HALD. But, this trend could be inhibited effectively over 1.5% Pd–WN/SBA-15. Consequently, WN in the catalysts plays an important role in determining the course of CAL hydrogenation in terms of both the rate and the selectivity toward either C=C or C=O hydrogenation.

It has been proven that all HALC produced on Pd catalyst is entirely produced through the further hydrogenation of the COL rather than HALD for the hydrogenation of CAL.<sup>[34,35]</sup> Thus, the higher selectivity to HALC indicates that there is much COL formed over the 1.5% Pd/SBA-15 by the hydrogenation of C=O firstly, which is then hydrogenated to HALC immediately. Little COL was detected during the process because COL hydrogenation to HALC was 30 times faster than the hydrogenation of CAL to COL on Pd.<sup>[34,35]</sup> It is well known the aldehyde reactant

**Table 3.** Hydrogenation of cinnamaldehyde over different catalysts.<sup>[a]</sup>

| Sample                                 | Conversion [%] | TOF [ $\text{h}^{-1}$ ] <sup>[b]</sup> | Selectivity [%] |     |      |                       |
|--|----------------|--|-----------------|-----|------|-----------------------|
|  |                |  | HALD            | COL | HALC | Others <sup>[c]</sup> |
| WN/SBA-15                              | 6.9            | –                                      | 7.6             | 3.2 | 0    | 89.2                  |
| 0.75% Pd/SBA-15                        | 42.5           | 451                                    | 54.9            | 2.5 | 24.3 | 18.3                  |
| 1.5% Pd/SBA-15                         | 76.9           | 418                                    | 51.5            | 0.8 | 38.9 | 8.8                   |
| 0.75% Pd–WN/SBA-15                     | 70.6           | 757                                    | 89.5            | 0.7 | 5.6  | 4.2                   |
| 1.5% Pd–WN/SBA-15                      | 99.5           | 532                                    | 97.6            | 0.4 | 1.1  | 0.9                   |
| 1.5% Pd– $\text{Mo}_2\text{N}$ /SBA-15 | 88.7           | 482                                    | 80.8            | 0.6 | 13.3 | 5.3                   |

[a] Reaction conditions: 50 mg catalyst, 1.00 g CAL, 30 mL isopropanol, 10 bar  $\text{H}_2$ , 313 K, 2 h. [b] Turnover frequency (TOF) = [(moles of cinnamaldehyde reacted)/[(moles of Pd loading) × (reaction time)]]. [c] Includes 1-(3-propoxyprop-1-enyl)benzene, cinnamyl formate, cinnamic acid, benzyl, cinnamate, 4,4-diphenylcyclohexa-1,5-dienyl acetate, and other condensation products that could not be identified by GC–MS because of their large molecular masses.

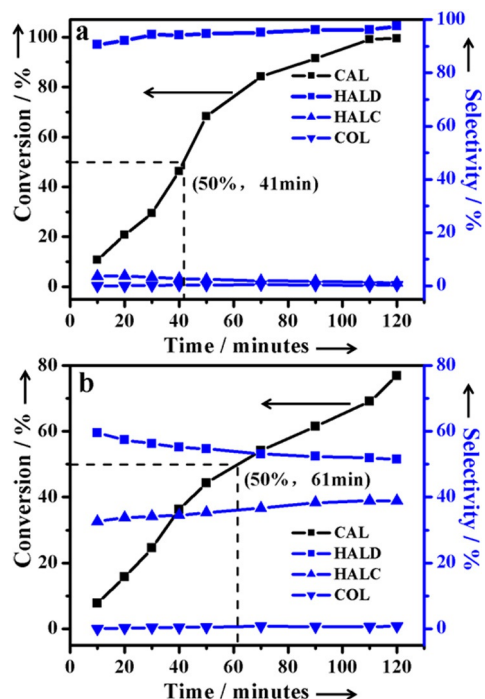


**Figure 7.** Selective hydrogenation of cinnamaldehyde catalyzed by a) 1.5% Pd-WN/SBA-15 and b) 1.5% Pd/SBA-15.

can be adsorbed on a metal surface in a flat, planar adsorption mode, parallel to the surface with both C=C and C=O bonds involved in adsorption and in the mode of the carbonyl group (C=O).<sup>[5]</sup> The former adsorption mode favors the hydrogenation of C=C yielding HALD, whereas the latter facilitates the hydrogenation of C=O to produce COL.<sup>[36]</sup> It should be stressed out that metal particle size is an important feature that could influence the selectivity toward saturated aldehyde, and smaller particles of Pt, Pd, Ru, and Co result in higher selectivity to C=C hydrogenation. This particle size effect of the metal was connected to the phenyl group, sterically hampering the approach of the cinnamaldehyde molecule parallel to a flat metal surface because of the steric repulsion of the aromatic ring.<sup>[5]</sup> However, this steric effect does not operate on small particles on which both the C=C and C=O bonds absorb on the surface. Thus, this increased selectivity on the 1.5% Pd-WN/SBA-15 is ascribed to that the small Pd NPs promote the absorption of CAL with both the C=C and C=O bonds, which facilitates the hydrogenation of the C=C bond to HALD. However, for 1.5% Pd/SBA-15 with relatively large Pd NPs, the parallel absorption is inhibited and the CAL can absorb by its C=O group to form COL, which is further hydrogenated to HALC immediately. Therefore, 1.5% Pd-WN/SBA-15 performs constantly increasing selectivity to HALD and much lower selectivity to HALC.

More detailed kinetic runs of the CAL hydrogenation were conducted over 1.5% Pd-WN/SBA-15. The kinetic curves of CAL hydrogenation under different temperature (298, 308, 313, and 323 K) and corresponding Arrhenius plots are displayed in Figure 8. To extract the activation energy of CAL hydrogenation, the data were gained at low conversions (<30%). As shown in Figure 8a, plotting ln[CAL] against time showed

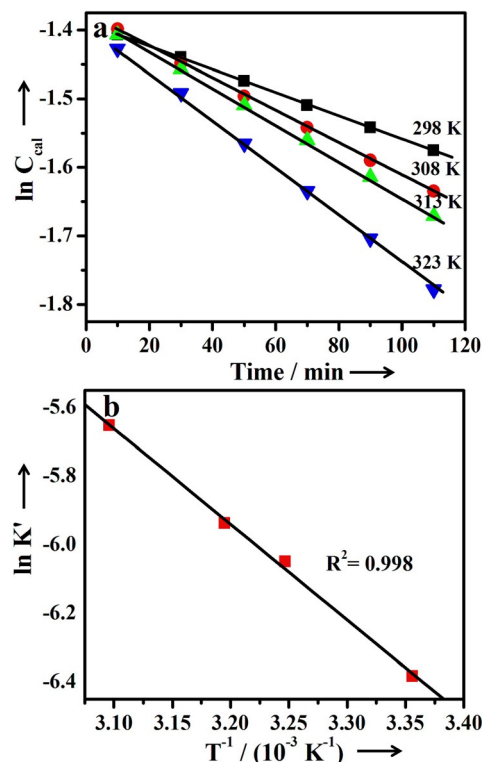


**Figure 8.** a) Plot of ln[CAL] versus reaction time for the conversion of CAL on 1.5% Pd-WN/SBA-15 at four different temperatures. b) Arrhenius plot of the pseudo-first-order rate constants extracted from the data shown in (a). Reaction conditions: 10 bar H<sub>2</sub>, 800 rpm stirring speed, 1.0 g CAL, 18 mg 1.5% Pd-WN/SBA-15, 30 mL isopropanol.

a straight line. This indicates that the reaction rate fits to the first-order reaction, consistent with others.<sup>[12,37]</sup> Arrhenius equation of the pseudo-first-order reaction constants was used to calculate an apparent activation energy ( $E_a$ ) at four different temperatures (Figure 8b). The  $E_a$  of 23.2 kJ mol<sup>-1</sup> was obtained over 1.5% Pd-WN/SBA-15 in our case, which is lower than that of the 1.5% Pd/SBA-15 (29.1 kJ mol<sup>-1</sup>, Figure S5). Thus, it is clearly confirmed that the synergistic effect between Pd and WN does suppress the activation barrier of hydrogenation. These results evidently depict the superiority of 1.5% Pd-WN/SBA-15 over the 1.5% Pd/SBA-15 in respect to the catalytic rate. The enhanced activity and reaction rate may be contributed to the decreased Pd NPs size and the modified electronic structure of the surface Pd on 1.5% Pd-WN/SBA-15, which originated from the intensive interaction of Pd and WN.<sup>[33,38]</sup>

The stability of the catalysts was also investigated in the selective hydrogenation of CAL over the 1.5% Pd-WN/SBA-15 and 1.5% Pd/SBA-15. To our delight, the 1.5% Pd-WN/SBA-15 still maintained its original activity after the fifth run, and the selectivity to HALD also showed no distinct loss within five reaction cycles (Figure 9). After the fifth cycle, only negligible Pd was leached for the 1.5% Pd-WN/SBA-15 catalyst as detected by ICP-OES (Table 1). The TEM image of the used 1.5% Pd-WN/SBA-15 (Figure S6) after the fifth run was almost the same as that of the fresh catalyst, suggesting that it is aggregation-free of Pd, which is consistent with the result of XRD pattern (Figure S7). The XPS spectra also suggest that the electronic

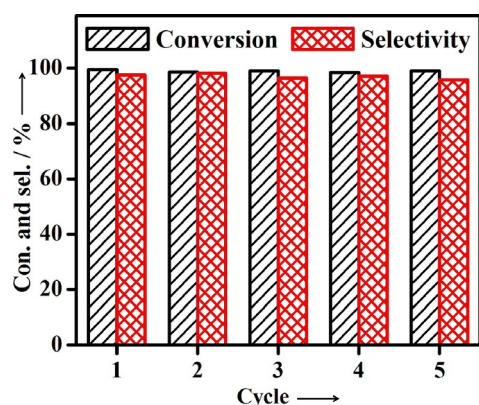


**Figure 9.** Stability test for the 1.5% Pd-WN/SBA-15 shown as performance versus number of recycling runs. Reaction conditions: 50 mg 1.5% Pd-WN/SBA-15, 1.00 g CAL, 30 mL isopropanol, 10 bar H<sub>2</sub>, 313 K, 2 h.

state and ratio of the Pd species on the surface of the fifth reused catalyst are similar to that of the fresh catalyst (Figure S8, Table 2). Nevertheless, the 1.5% Pd/SBA-15 performed a noticeable decrease of CAL conversion during the recycling (Figure S9). At the fourth cycle, only 48.3% CAL conversion was obtained. Thus, the existence of WN clearly benefits to improve the stability of the catalyst.

To further investigate the versatility of the 1.5% Pd-WN/SBA-15 catalyst, various unsaturated aldehydes were used as substrates under optimized conditions, and these results are listed in Table 4. It was found that hydrogenation of various  $\alpha,\beta$ -unsaturated aldehydes over the 1.5% Pd-WN/SBA-15 could obtain the corresponding saturated aldehydes with high selectivity and conversion. In view of the results, it indicates that steric effects induced by the substituent groups on the C atoms in the C=C bond have an influence on the intramolecular selectivity.

## Conclusions

The catalysts were prepared by loading Pd on different supports modified by small-size WN, and their catalytic performan-

ces were investigated for the chemoselective hydrogenation of cinnamaldehyde (CAL) on the C=C bond. It was found that modification of WN on the support improved the catalytic performance of Pd as a result of the synergistic effect between WN and Pd. Among these catalysts, Pd-WN/SBA-15 displayed the highest yield of hydrocinnamaldehyde (HALD, 97.1%), moreover, it was reused five times successively without significant loss of catalytic activity and selectivity. The reaction kinetics has been represented by a standard pseudo-first-order approximation, which indicates that the activation energy is lower over Pd-WN/SBA-15 (23.2 kJ mol<sup>-1</sup>) than over Pd/SBA-15 (29.1 kJ mol<sup>-1</sup>). The enhancement is attributed to the synergistic effect of Pd and WN, which enriches the electron density of Pd by transferring electrons from WN to Pd, increases the ratio of Pd<sup>0</sup> species, and decreases the Pd size on the Pd-WN/SBA-15 catalyst. This synergistic effect between Pd and WN also reduces the usage of Pd to enhance the catalytic efficiency in some extent. Furthermore, hydrogenation of various  $\alpha,\beta$ -unsaturated aldehydes over the 1.5% Pd-WN/SBA-15 could obtain the corresponding saturated aldehydes with high selectivity and conversion. Thus, it opens a new way to design many more powerful catalysts by interaction between noble metal and nitrides and lessen the usage of noble metal in catalysis field.

## Experimental Section

### Catalyst preparation

SBA-15 was prepared with the triblock copolymer Pluronic P123 and tetraethylorthosilicate (TEOS) according to a typical synthesis route.<sup>[20]</sup> The synthesis of other supports is described in the Supporting Information, including MCM-41, Al<sub>2</sub>O<sub>3</sub>, SAPO-34 and NaBeta.

The preparation is described for the Pd-WN/SBA-15 catalyst as example; the other catalysts were synthesized accordingly. As shown in Scheme 2, the WN/SBA-15 composite was prepared by anchoring H<sub>4</sub>[Si(W<sub>3</sub>O<sub>10</sub>)<sub>4</sub>] cluster on *N*-[3-(trimethoxysilyl)propyl]-ethylenediamine modified SBA-15 (SBA-15-NH<sub>2</sub>), and followed by calcination in NH<sub>3</sub>. A typical procedure was as follow: SBA-15 (2.0 g) was added to the mixed solution containing *N*-[3-(trimethoxysilyl)propyl] ethylenediamine (4.0 mL) and ethanol (4.0 mL). After stirring for

| Entry | Substrate   | Product   | <i>t</i> [h] | Conversion [%] <sup>[b]</sup> | Selectivity [%] <sup>[b]</sup> |
|-------|---|---|--------------|-------------------------------|--------------------------------|
| 1     |  |  | 0.5          | 80.7                          | 70.1                           |
| 2     |  |  | 2.5          | 89.7                          | 85.3                           |
| 3     |  |  | 2            | 99.5                          | 97.1                           |
| 4     |  |  | 2            | 94.3                          | 85.4                           |
| 5     |  |  | 3            | 76.5                          | 77.0                           |
| 6     |  |  | 5            | 95.3                          | 83.9                           |

[a] Reaction conditions: 50 mg 1.5% Pd-WN/SBA-15, 1.00 g substrate, 30 mL isopropanol, 10 bar H<sub>2</sub>, 313 K. [b] Determined by GC and GC-MS.



**Scheme 2.** Synthetic scheme for the construction of the ternary Pd-WN/SBA-15 catalyst.

24 h, the excess *N*-[3-(trimethoxysilyl)propyl]-ethylenediamine was removed by washing with ethanol. Finally, the SBA-15-NH<sub>2</sub> was obtained followed by drying at 333 K for several hours (step 1). Subsequently, SBA-15-NH<sub>2</sub> (0.50 g) was pretreated in an oven at 473 K for 2 h, and then was impregnated with the solution (10 mL containing 0.05 g SiW<sub>12</sub>). After stirring for 6 h, the mixture was filtered and washed. After drying at 333 K for 12 h, the precursor SiW<sub>12</sub>/SBA-15-NH<sub>2</sub> (step 2) was heated at 793 K with a heating rate of 3 K min<sup>-1</sup> and maintained for 3 h under pure NH<sub>3</sub> (80 mL min<sup>-1</sup>). After slowly cooling to RT under a N<sub>2</sub> atmosphere, the WN/SBA-15 composite was obtained (step 3).

The ternary Pd-WN/SBA-15 was formed by loading Pd on WN/SBA-15 composite by a sodium borohydride (NaBH<sub>4</sub>) method (step 4).<sup>[39,40]</sup> Typically, a certain amount of PdCl<sub>2</sub> solution (10 mmol L<sup>-1</sup>) and WN/SBA-15 composite (0.30 g) were dissolved in distilled water (10 mL), and the mixture was stirred for 12 h. 1 M NaOH was added to adjust the pH of the solution to ≈ 10. Then, a certain amount of NaBH<sub>4</sub> solution (0.2 mol L<sup>-1</sup>) was added to this suspension, and the molar ratio of NaBH<sub>4</sub> to PdCl<sub>2</sub> was 5. Finally, Pd-WN/SBA-15 was separated by filtrations, washed with distilled water and absolute ethanol in sequence and dried at 333 K overnight in a vacuum oven. The theoretical content of Pd was 1.5% and 0.75% and the catalysts were denoted as 1.5% Pd-WN/SBA-15 and 0.75% Pd-WN/SBA-15, respectively. As references, Pd supported on SBA-15 with 1.5% Pd content was also prepared under the similar conditions, which was denoted as 1.5% Pd/SBA-15.

### Catalyst characterization

Wide-angle X-ray diffraction (XRD) of the catalysts was recorded in the 2θ range of 10–80° on a Bruker D8 Advance X-ray diffractometer with Cu Kα (λ = 1.5418 Å) radiation (40 kV, 40 mA). As for the small-angle XRD, the scan range was 0.5–5°, and the scanning rate was 1° min<sup>-1</sup>. Nitrogen adsorption-desorption isotherms were collected on a Micromeritics Tristar 3020 surface area and a porosimetry analyzer for mesoporous materials at 77 K. The BET equation was used to calculate the specific surface area. Pore size distributions were obtained using the Barrett-Joyner-Halenda (BJH) method from the adsorption branch of the isotherm. SEM mapping was analyzed by scanning electron microscopy (SEM: Hitachi S-4800) with an acceleration voltage of 5 kV. TEM characterization and high-resolution TEM (HRTEM) were determined by using a JEM-2100 electron microscope (JEOL, Japan) with an acceleration voltage of 200 kV. Carbon-coated copper grids were used as the

sample holders. XPS measurements were performed on a Kratos-AXIS ULTRA DLD with an Al Kα radiation source. The binding energies (BE) of elements were referenced to the C 1s peak at 284.8 eV. The content of palladium and tungsten nitride was determined by ICP-OES, which was performed by a PerkinElmer Optima 7000DV analyzer. Before the measurement, each sample was dissolved in a diluted HF and chloroazotic acid solution. The content of tungsten nitride was also analyzed by X-ray fluorescence spectrometry using a Bruker S4 Explorer instrument.

### Selective hydrogenation of cinnamaldehyde

In a typical reaction, cinnamaldehyde (1.0 g), catalyst (50 mg), and isopropanol (30 mL) were precharged in a 100 mL autoclave. The autoclave was purged with N<sub>2</sub> three times at 5 bar and H<sub>2</sub> three times at 5 bar to remove air, and the mixture was then magnetically stirred at 800 rpm under 10 bar of H<sub>2</sub> at 313 K for 2 h. After the reaction, the products were analyzed by GC (Agilent 7820A) with flame ionization detection and a HP-5 capillary column (30 m × 0.32 mm × 0.25 mm). Benzyl alcohol was used as an internal standard. The products were further identified by GC-MS (Agilent 6890/5973N). For the test of the stability, the catalyst used above was recovered by centrifugation, washed three times with isopropanol, and then used for the next run without any further treatment.

### Acknowledgements

This work was financially supported by the National Natural Science Foundation of China (No. 21371053, 21401048, 21571054), the China Postdoctoral Science Special Foundation (No. 2015T80374), International Science & Technology Cooperation Program of China (2014DFR41110), Natural Sciences Fund of Heilongjiang Province (B2015009), the Application technology research and development projects in Harbin (2013AE4BW051), Innovative Research Project of Key Laboratory of Functional Inorganic Material Chemistry (Heilongjiang University), Ministry of Education.

**Keywords:** electron transfer · hydrogenation · nitrides · palladium · tungsten

- [1] K. Bauer, D. Garbe, *Common Fragrance and Flavor Materials*, VCH, Weinheim, 1985.
- [2] H. G. Manyar, B. Yang, H. Daly, H. Moor, S. McMonagle, Y. Tao, G. D. Yadav, A. Goguet, P. Hu, C. Hardacre, *ChemCatChem* **2013**, *5*, 506–512.
- [3] H. L. Liu, L. N. Chang, L. Y. Chen, Y. W. Li, *ChemCatChem* **2016**, *8*, 946–951.
- [4] T. Szumelda, A. Drelinkiewicz, R. Kosydar, J. Gurgul, *Appl. Catal. A* **2014**, *487*, 1–15.
- [5] P. Gallezot, D. Richard, *Catal. Rev. Sci. Eng.* **1998**, *40*, 81–126.
- [6] J. J. Shi, M. Y. Zhang, W. C. Du, W. S. Ning, Z. Y. Hou, *Catal. Sci. Technol.* **2015**, *5*, 3108–3112.
- [7] K. R. Kahsar, D. K. Schwartz, J. W. Medlin, *J. Mol. Catal. A* **2015**, *396*, 188–195.
- [8] M. Bidaoui, C. Espedel, S. Sabour, L. Benatallah, N. Saib-Bouchenafa, S. Royer, O. Mohammedi, *J. Mol. Catal. A* **2015**, *399*, 97–105.
- [9] Z. B. Tian, Q. Y. Li, Y. Li, S. Y. Ai, *Catal. Commun.* **2015**, *61*, 97–101.
- [10] X. W. Ji, X. Y. Niu, B. Li, Q. Han, F. L. Yuan, F. Zaera, Y. J. Zhu, H. G. Fu, *ChemCatChem* **2014**, *6*, 3246–3253.
- [11] Z. Guo, Y. T. Chen, L. S. Li, X. M. Wang, G. L. Haller, Y. H. Yang, *J. Catal.* **2010**, *276*, 314–326.

- [12] X. Yang, D. Chen, S. J. Liao, H. Y. Song, Y. W. Li, Z. Y. Fu, Y. L. Su, *J. Catal.* **2012**, *291*, 36–43.
- [13] T. Szumelda, A. Drelinkiewicz, R. Kosydar, J. Gurgul, *Appl. Catal. A* **2014**, *487*, 1–15.
- [14] J. S. J. Hargreaves, *Coord. Chem. Rev.* **2013**, *257*, 2015–2031.
- [15] W. F. Chen, J. T. Muckerman, E. Fujita, *Chem. Commun.* **2013**, *49*, 8896–8909.
- [16] D. A. Ruddy, J. A. Schaidle, J. R. Ferrell, J. Wang, L. Moens, J. E. Hensley, *Green Chem.* **2014**, *16*, 454–490.
- [17] H. J. Yan, C. G. Tian, L. Sun, B. Wang, L. Wang, J. Yin, A. P. Wu, H. G. Fu, *Energy Environ. Sci.* **2014**, *7*, 1939–1949.
- [18] J. Yin, L. Wang, P. Yu, L. Zhao, C. G. Tian, B. J. Jiang, D. D. Zhao, W. Zhou, H. G. Fu, *ChemElectroChem* **2015**, *2*, 1813–1820.
- [19] D. Wang, Y. J. Zhu, C. G. Tian, L. Wang, W. Zhou, Y. L. Dong, Q. Han, Y. F. Liu, F. L. Yuan, H. G. Fu, *Catal. Sci. Technol.* **2016**, *6*, 2403–2412.
- [20] D. Y. Zhao, J. L. Feng, Q. S. Huo, N. Melosh, G. H. Fredrickson, B. F. Chmelka, G. D. Stucky, *Science* **1998**, *279*, 548–552.
- [21] A. Pineda, A. M. Balu, J. M. Campelo, A. A. Romero, D. Carmona, F. Balas, J. Santamaria, R. Luque, *ChemSusChem* **2011**, *4*, 1561–1565.
- [22] M. Ojeda, A. M. Balu, V. Barrón, A. Pineda, A. García, A. A. Romero, R. Luque, *J. Mater. Chem. A* **2014**, *2*, 387–393.
- [23] A. Kafizas, C. J. Carmalt, I. P. Parkin, *Coord. Chem. Rev.* **2013**, *257*, 2073–2119.
- [24] M. S. Bazarjani, M. M. Müller, H. J. Kleebe, C. Fasel, R. Riedel, A. Gurlo, *J. Mater. Chem. A* **2014**, *2*, 10454–10464.
- [25] S. Abate, P. Lanzafame, S. Perathoner, G. Centi, *Catal. Today* **2011**, *169*, 167–174.
- [26] X. Yang, L. Du, S. Liao, Y. Li, H. Song, *Catal. Commun.* **2012**, *17*, 29–33.
- [27] S. T. Oyama, *J. Solid State Chem.* **1992**, *96*, 442–445.
- [28] R. H. Wang, Y. Xie, K. Y. Shi, J. Q. Wang, C. G. Tian, P. K. Shen, H. G. Fu, *Chem. Eur. J.* **2012**, *18*, 7443–7451.
- [29] V. Z. Radkevich, T. L. Senko, K. Wilson, L. M. Grishenko, A. N. Zaderko, V. Y. Diyuk, *Appl. Catal. A* **2008**, *335*, 241–251.
- [30] J. Yang, Y. Xie, R. H. Wang, J. B. Jiang, C. G. Tian, G. Mu, J. Yin, B. Wang, H. G. Fu, *ACS Appl. Mater. Interfaces* **2013**, *5*, 6571–6579.
- [31] W. Chen, Z. Fan, X. Pan, X. Bao, *J. Am. Chem. Soc.* **2008**, *130*, 9414–9419.
- [32] X. Pan, X. Bao, *Acc. Chem. Res.* **2011**, *44*, 553–562.
- [33] Z. Z. Wei, Y. T. Gong, T. Y. Xiong, P. F. Zhang, H. R. Li, Y. Wang, *Catal. Sci. Technol.* **2015**, *5*, 397–404.
- [34] A. Hammoudeh, S. Mahmoud, *J. Mol. Catal. A* **2003**, *203*, 231–239.
- [35] G. R. Cairns, R. J. Cross, D. Stirling, *J. Catal.* **1997**, *166*, 89–97.
- [36] P. Claus, *Top. Catal.* **1998**, *5*, 51–62.
- [37] W. O. Oduro, N. Cailuo, K. M. K. Yu, H. W. Yang, S. C. Tsang, *Phys. Chem. Chem. Phys.* **2011**, *13*, 2590–2602.
- [38] X. Yang, L. P. Wu, L. L. Ma, X. J. Li, T. J. Wang, S. J. Liao, *Catal. Commun.* **2015**, *59*, 184–188.
- [39] Y. Li, X. Xu, P. Zhang, Y. Gong, H. Li, Y. Wang, *RSC Adv.* **2013**, *3*, 10973–10982.
- [40] Y. Wang, J. Yao, H. R. Li, D. S. Su, M. Antonietti, *J. Am. Chem. Soc.* **2011**, *133*, 2362–2365.

---

Received: February 16, 2016

Published online on April 18, 2016